# Extended Kalman filter for estimating aircraft orientation from velocity measurements

L.M. Ehrman and A.D. Lanterman

**Abstract:** A coordinated flight model for estimating the orientation of an aircraft under track from velocity measurements into an extended Kalman filter (EKF) framework is placed here. In doing so, it makes two contributions. First, the EKF provides a rigorous framework for addressing this problem, blending modelling error and measurement error. Second, the EKF supplements the estimated orientation with a measure of the uncertainty in that estimate. Such estimates of uncertainty are crucial in a number of applications, including using the orientation estimates to approximate the radar cross section of the aircraft under track, in an attempt to identify targets. The EKF's performance is demonstrated using both a straight-and-level manoeuvre and a complicated manoeuvre recorded on-board a manoeuvring F-15. In both cases, the state estimates of the EKF are similar to the results obtained from a coordinated flight model. The true orientations almost always fall within one standard deviation of the estimates, as determined by the estimated covariance.

## 1 Introduction

A number of problems require that an aircraft's orientation be estimated from position and/or velocity measurements. For example, recent work [1] has attempted to identify aircraft under track by comparing the radar cross section (RCS) of the aircraft to an RCS database housing data for several varieties of targets. To access the RCS database, the incident and observed angles on the aircraft must be known. These can easily be computed if the sensor positions are known, as well as the target's position and orientation. Some tracking applications may also benefit from estimates of the target's orientation to better predict the target's state. Thus, although the work in this paper is applied to a target recognition application that uses passive radar, it could easily be applied to many other problems.

Coordinated flight models are typically applied to position and/or velocity measurements to estimate an aircraft's orientation. However, these coordinated flight models have two major limitations. First, they neglect measurement noise, essentially assuming that the measurements are exactly known. Second, they fail to provide an estimate of the uncertainty associated with the estimated orientation.

This paper combats these limitations by embedding a coordinated flight model for estimating aircraft orientation from velocity measurements, described in Section 2, into an extended Kalman filter (EKF), developed in Section 3. Since a passive radar application (using illuminators of opportunity) is used to demonstrate this technique, the velocity measurements are assumed to come from an EKF much like the one developed by Howland [2, 3]. Nevertheless, this EKF for estimating aircraft orientation could just as easily apply to trackers providing measurements from a number of sources, including those obtained from traditional radar sensors. The EKF that estimates aircraft orientation accounts for measurement error and blends it with the modelling error (i.e. the error that would occur even if the measurements were perfectly known). In addition to providing a state estimate (where the state is the aircraft's orientation), the EKF also estimates the covariance associated with the state. Thus, the EKF solves both problems associated with the use of the basic coordinated flight model. Results are given for simple and complex trajectories in Section 4. In both cases, the truth values fall within one standard deviation (as computed from the state covariance matrix of the EKF) of the state estimates.



doi:10.1049/iet-rsn:20070025

Paper first received 13th February 2006 and in revised form 16th February 2007

The authors are with the School of Electrical and Computer Engineering, Georgia Institute of Technology, Mail Code 0250, Atlanta, GA 30332, USA

E-mail: lisa_m_ehrman@yahoo.com

## 2 Coordinated flight model

The conventions used for orientation are depicted in Fig. 1. Let the $p_X$–$p_Y$–$p_Z$ coordinate frame be a Cartesian grid whose origin is some point on the Earth's surface near the location of the aircraft. As is fairly standard, yaw, the first element of the orientation vector, is defined to be the rotation about the vector coming out the top of the aircraft. It is measured relative to the $p_X$–$p_Y$–$p_Z$ coordinate frame such that a yaw of $0^\circ$ corresponds to an aircraft flying down the $+p_X$-axis, and a yaw of $90^\circ$ etc corresponds to an aircraft flying down the $+p_Y$-axis. Pitch, the second element, is the rotation about the vector extending out the wing of the aircraft, and the third element, roll, is the rotation about the vector in the direction of the aircraft's nose [4].

### 2.1 Estimating yaw

Using the coordinated flight model, the yaw is modelled as a function of the aircraft motion in the $p_X$–$p_Y$ plane, and is expressed by

$$\psi = \arctan\left(\frac{v_Y}{v_X}\right) \tag{1}$$

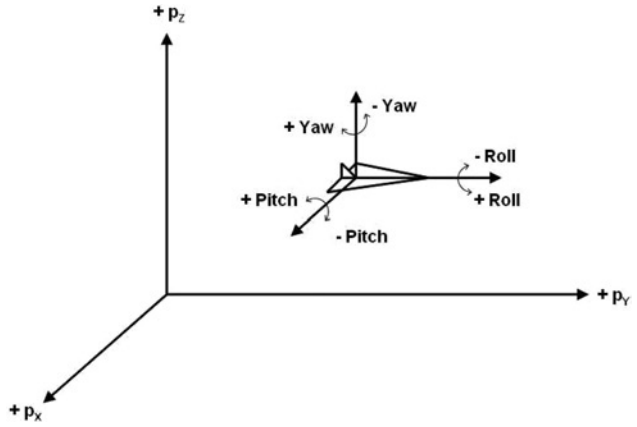


**Fig. 1** *Coordinate convention*

where $\boldsymbol{v}_X$ and $\boldsymbol{v}_Y$ are the $p_X$ and $p_Y$ components of the velocity vector [5].

### 2.2 Estimating pitch

As should be clear from Fig. 1, the aircraft's pitch describes the angle between the total velocity vector and the velocity vector in the $p_X$–$p_Y$ plane, and can be thought of as the angle at which the aircraft is changing altitude. Let ($\boldsymbol{v}_X$, $\boldsymbol{v}_Y$, $\boldsymbol{v}_Z$) denote the aircraft's velocity. The pitch is then approximated under the coordinated flight model as

$$\theta = \arctan\left(\frac{\boldsymbol{v}_Z}{\sqrt{\boldsymbol{v}_X^2 + \boldsymbol{v}_Y^2}}\right) \tag{2}$$

As long as the sampling rate of the aircraft's position is on the order of seconds, this linear approximation of the pitch is sufficiently accurate for our purposes [5].

### 2.3 Estimating roll

Under the coordinated flight model [5] and L. Ehrman and A.D. Lanterman (submitted data), the aircraft's roll, which is the rotation about the vector extending through the aircraft's nose, is approximated by

$$|\phi| = \arctan\left(\frac{|\boldsymbol{v}|^2 \cos(\theta)}{R_X g}\right) \tag{3}$$

where $|v|$ is the magnitude of the aircraft's velocity and $g$ is the standard gravity at Earth's surface; $R_{XY}$ is the radius of curvature of the aircraft's turn, computed with

$$R_{XY}(t) = \frac{[\boldsymbol{v}_x(t)^2 + \boldsymbol{v}_y(t)^2]^{3/2}}{\boldsymbol{v}_x(t)a_y(t) - a_x(t)\boldsymbol{v}_y(t)} \tag{4}$$

where $v_x$ and $v_y$ are the $x$ and $y$ components of velocity and $a_x$ and $a_y$ are the $x$ and $y$ components of acceleration. Two points are worth mentioning. First, $R_{XY}$ must be computed in the plane in which the aircraft has zero pitch, rather than in the coordinate system in which the $p_x$–$p_y$ plane corresponds to the ground plane [5]. A second caveat is that only the magnitude of the roll is observable using (3). Because the expression for roll given by (3) is a function of the magnitude of the velocity, the radius of acceleration, and the pull of gravity, it always results in a positive roll angle. From Fig. 1, it is clear that positive roll angles are associated with rolls in which the aircraft's right wing is down. If the aircraft is flying in a clockwise manner, then the roll angle should be positive, given the current convention. Conversely, counter-clockwise flight should result in negative roll angles.

A simple way to implement this convention is to test for counter-clockwise flight, and invert the sign of the roll angle when it is detected. A logical test for counter-clockwise flight in a certain incremental period of time, d$t$, is given by

$$[(\mathrm{d}x < 0)\,\text{and}\,(\text{CU})] \quad \text{or} \quad [(\mathrm{d}x > 0)\,\text{and}\,(\text{CD})] \tag{5}$$

where CU denotes a flight path that is concave-up (as plotted in the $p_x$–$p_y$ plane) during d$t$, CD denotes a flight path that is concave-down (as plotted in the $p_x$–$p_y$ plane) during d$t$ and d$x$ is the incremental distance traversed by the aircraft in the $p_x$-direction during d$t$. Applying this test to the values computed with (3), results in the computation of aircraft roll in accordance with the conventions selected in Fig. 1.

### 2.4 Limitations of the coordinated flight model

This coordinated flight model has two major limitations. First, by assuming that the aircraft nose is pointed exactly in the direction of motion, the model neglects 'crabbing'. This condition, which often occurs in conjunction with high wind or severe weather, is characterised by a difference in the $p_X$–$p_Y$ plane between the direction of the aircraft's nose and the direction of the aircraft's motion. The more serious limitation of the model is that it only provides a state estimate, and makes no attempt to model the uncertainty associated with each estimate.

## 3 EKF for estimating aircraft orientation from velocity measurements

This section combats the limitations of the coordinated flight model by developing it into an EKF for estimating aircraft orientation from velocity estimates. Consider the two distinct types of error present in this problem. Measurement error, as the name implies, is the error on the velocity measurements received from the tracker. Modelling error is also present, and can be thought of as the error that would occur even if the measurements were perfectly known. The basic coordinated flight model from Section 2 treats the measurements as though they are perfectly known and provides no estimate of the uncertainty resulting from modelling error. The EKF, in contrast, balances both types of errors to estimate the target's state and covariance. Furthermore, the EKF accounts for 'crabbing' and other modelling errors through the process noise and (optional) covariance inflation. In doing so, the EKF sidesteps both limitations of the coordinated flight model.

### 3.1 EKF model

Our development of an EKF that estimates the aircraft orientation from velocity estimates begins with the assumption that the state model is a constant-velocity trajectory (relative to the $p_X$–$p_Y$–$p_Z$ coordinate frame), described by

$$x_k = x_{k-1} + q_k \tag{6}$$

where $q_k$ is the process noise term, modelled as a zero-mean Gaussian random variable with covariance $Q_k$. The state at time $k$, denoted as $x_k$, is a vector consisting of the target's yaw, pitch and roll.

The measurement model is then described by

$$z_k = \boldsymbol{h}_k(x_k) + s_k \tag{7}$$

where $z_k$ is the measurement vector at time $k$ consisting of the $p_X$, $p_Y$ and $p_Z$ components of the target's velocity, $\boldsymbol{h}_k(x_k)$ is a nonlinear mapping of the state into the measurement space and $s_k$ is the measurement noise term, modelled as a zero-mean Gaussian random variable with covariance $S_k$.

The standard EKF equations are given next, to clarify notation. The state, $x_{k-1|k-1}$, and its covariance, $P_{k-1|k-1}$, are extrapolated from time $t_{k-1}$ to time $t_k$ with

$$x_{k|k-1} = \boldsymbol{F}_k x_{k-1|k-1} \tag{8}$$

and

$$P_{k|k-1} = \boldsymbol{F}_k P_{k-1|k-1} \boldsymbol{F}_k^{\mathrm{T}} + Q_k \tag{9}$$

Given the state model, it follows that $\boldsymbol{F}_k = \boldsymbol{I}$. Thus, the time-update equations for this EKF reduce to

$$x_{k|k-1} = x_{k-1|k-1} \tag{10}$$

and

$$P_{k|k-1} = P_{k-1|k-1} + Q_k \tag{11}$$

As is standard practice [6], the process noise, $Q_k$, is selected to tune the filter to the application.

The measurement update equations are then computed using

$$K_k = P_{k|k-1} \boldsymbol{H}_k (\boldsymbol{H}_k P_{k|k-1} \boldsymbol{H}_k^{\mathrm{T}} + S_k)^{-1} \tag{12}$$

$$x_{k|k} = x_{k|k-1} + K_k (z_k - \boldsymbol{h}_k(x_{k|k-1})) \tag{13}$$

and

$$P_{k|k} = (I - K_k \boldsymbol{H}_k) P_{k|k-1} \tag{14}$$

where $\boldsymbol{H}_k$ is the linearisation of the nonlinear mapping $\boldsymbol{h}_k(x_{k|k-1})$ [Note 1]. Our training data are admittedly limited. One path for future work is to re-tune the filter using a more extensive set of training data. This completes one update cycle in the EKF.

Although EKFs are quite common, initialising them is often something of an art. One advantage of this EKF is that the initialisation procedure flows very naturally from its development. No exotic algorithms are required. Rather, the state vector of this EKF is simply initialised using the coordinated flight model.

### 3.2 Solving for **h** and **H** in the general case

Solving for $\boldsymbol{h}_k(x_{k|k-1})$ and $\boldsymbol{H}_k$ is far from trivial. First, it is necessary to solve for the $x$, $y$ and $z$ components of the target's velocity, which comprise the measurement, in terms of the yaw, pitch and roll, which comprise the state. To make this problem mathematically tractable, the radius of curvature is computed from the measurements via (4), and is treated as noiseless in this derivation. Note that it is not necessary to wait until the entire trajectory has been collected to compute $R_{XY}$. Rather, it is only necessary to wait for two measurements, thus allowing for updated velocity and acceleration measurements, to compute $R_{XY}$. For example, $R_{XY}(t)$ can be computed using measurments through time $t + 2\Delta_t$, where $\Delta_t$ is the time between measurements. Note that hereafter we will drop the subscript $XY$ from $R_{XY}$ for notational compactness.

Note 1: As is often the practice when implementing EKFs, the covariance is inflated following the measurement update step to further account for measurement error. Determining whether this is necessary and how much inflation is required are questions typically addressed through analysis of multiple sets of training data.

Solving (1) for $\boldsymbol{v}_Y$ results in

$$\boldsymbol{v}_Y = \boldsymbol{v}_X \tan(\psi) \tag{15}$$

Similarly, solving (2) for $\boldsymbol{v}_Z$ results in

$$\boldsymbol{v}_Z = \sqrt{\boldsymbol{v}_X^2 + \boldsymbol{v}_Y^2} \tan(\theta) \tag{16}$$

From (15), it follows that

$$\boldsymbol{v}_X^2 + \boldsymbol{v}_Y^2 = \boldsymbol{v}_X^2 + \boldsymbol{v}_X^2 \tan^2(\psi) \tag{17}$$

which reduces to

$$\boldsymbol{v}_X^2 + \boldsymbol{v}_Y^2 = \boldsymbol{v}_X^2 \sec^2(\psi) \tag{18}$$

Using this result, reduces (16) to

$$\boldsymbol{v}_Z = \boldsymbol{v}_X \sec(\psi) \tan(\theta) \tag{19}$$

Equation (3) is then rewritten for $|\boldsymbol{v}|^2$, resulting in

$$|\boldsymbol{v}|^2 = Rg \sec(\theta) \tan(|\phi|) \tag{20}$$

From (18) and (19), $|\boldsymbol{v}|^2$ is also given by

$$|\boldsymbol{v}|^2 = \boldsymbol{v}_X^2 \sec^2(\psi) + (\boldsymbol{v}_X \sec(\psi) \tan(\theta))^2 \tag{21}$$

which reduces to

$$|\boldsymbol{v}|^2 = \boldsymbol{v}_X^2 \sec^2(\psi) \sec^2(\theta) \tag{22}$$

Substituting (22) into (20) and solving for $\boldsymbol{v}_X$ results in

$$\boldsymbol{v}_X = \cos(\psi) \sqrt{Rg \cos(\theta) \tan(|\phi|)} \tag{23}$$

This is then substituted back into (15) and (16) to solve for $\boldsymbol{v}_Y$ and $\boldsymbol{v}_Z$ in terms of $\psi$, $\theta$, $\phi$ and $R$. The set of equations that map the state vector into the measurement space are summarised by

$$\boldsymbol{h}(x) = \begin{bmatrix} \boldsymbol{v}_X \\ \boldsymbol{v}_Y \\ \boldsymbol{v}_Z \end{bmatrix} = \begin{bmatrix} \cos(\psi)\sqrt{Rg \cos(\theta) \tan(|\phi|)} \\ \sin(\psi)\sqrt{Rg \cos(\theta) \tan(|\phi|)} \\ \tan(\theta)\sqrt{Rg \cos(\theta) \tan(|\phi|)} \end{bmatrix} \tag{24}$$

The linearisation of this nonlinear mapping, used in (12) and (14), is described by

$$\boldsymbol{H} = \begin{bmatrix} \frac{\partial \boldsymbol{v}_X}{\partial \psi} & \frac{\partial \boldsymbol{v}_X}{\partial \theta} & \frac{\partial \boldsymbol{v}_X}{\partial \phi} \\ \frac{\partial \boldsymbol{v}_Y}{\partial \psi} & \frac{\partial \boldsymbol{v}_Y}{\partial \theta} & \frac{\partial \boldsymbol{v}_Y}{\partial \phi} \\ \frac{\partial \boldsymbol{v}_Z}{\partial \psi} & \frac{\partial \boldsymbol{v}_Z}{\partial \theta} & \frac{\partial \boldsymbol{v}_Z}{\partial \phi} \end{bmatrix} \tag{25}$$

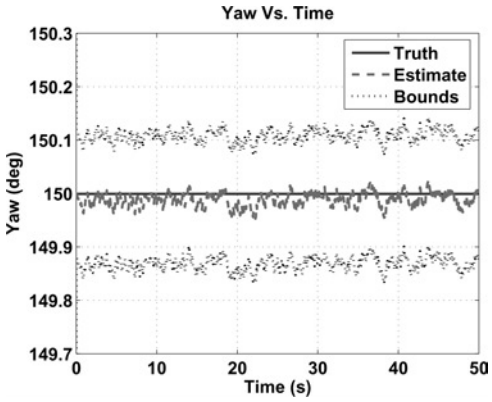


**Fig. 2** *Yaw estimated by the EKF: straight-and-level trajectory*

where the partial derivatives are given by

$$\frac{\partial \boldsymbol{v}_X}{\partial \psi} = -\sin(\psi)\sqrt{Rg\,\cos(\theta)\,\tan(|\phi|)} \tag{26}$$

$$\frac{\partial \boldsymbol{v}_Y}{\partial \psi} = \cos(\psi)\sqrt{Rg\,\cos(\theta)\,\tan(|\phi|)} \tag{27}$$

$$\frac{\partial \boldsymbol{v}_Z}{\partial \psi} = 0 \tag{28}$$

$$\frac{\partial \boldsymbol{v}_X}{\partial \theta} = \frac{-1}{2}\cos(\psi)\,\sin(\theta)\sqrt{Rg\,\sec(\theta)\,\tan(|\phi|)} \tag{29}$$

$$\frac{\partial \boldsymbol{v}_Y}{\partial \theta} = \frac{-1}{2}\sin(\psi)\,\sin(\theta)\sqrt{Rg\,\sec(\theta)\,\tan(|\phi|)} \tag{30}$$

$$\frac{\partial \boldsymbol{v}_Z}{\partial \theta} = \frac{-1}{2}\tan(\theta)\,\sin(\theta)\sqrt{Rg\,\sec(\theta)\,\tan(|\phi|)} + \sec^2(\theta)\sqrt{Rg\,\cos(\theta)\,\tan(|\phi|)} \tag{31}$$

$$\frac{\partial \boldsymbol{v}_X}{\partial \phi} = \frac{\cos(\psi)}{2\,\cos^2(|\phi|)}\sqrt{\frac{Rg\,\cos(\theta)}{\tan(|\phi|)}} \tag{32}$$

$$\frac{\partial \boldsymbol{v}_Y}{\partial \phi} = \frac{\sin(\psi)}{2\,\cos^2(|\phi|)}\sqrt{\frac{Rg\,\cos(\theta)}{\tan(|\phi|)}} \tag{33}$$

and

$$\frac{\partial \boldsymbol{v}_Z}{\partial \phi} = \frac{\tan(\theta)}{2\,\cos^2(|\phi|)}\sqrt{\frac{Rg\,\cos(\theta)}{\tan(|\phi|)}} \tag{34}$$

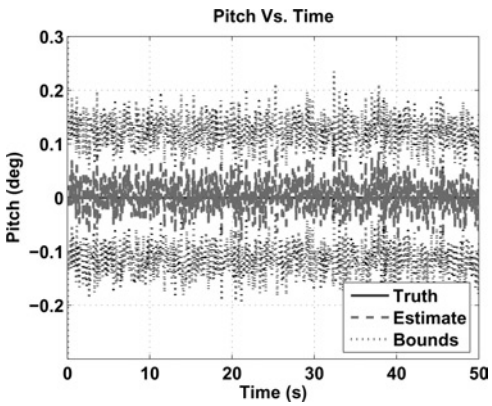


**Fig. 3** *Pitch estimated by the EKF: straight-and-level trajectory*

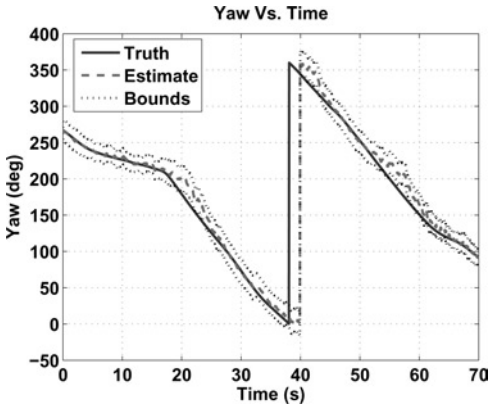


**Fig. 4** *Yaw estimated by the EKF: Edwards trajectory*

### 3.3 Numerical issues

Although the $\boldsymbol{H}$ matrix computed in Section 3.2 applies, in theory, to any target trajectory, it presents a numerical difficulty when the target follows a straight, constant-velocity trajectory in the $p_x$–$p_y$ plane. In such a case, the radius of curvature goes to infinity while the roll angle goes to zero. Thus, the product of $R$ and $\tan(|\phi|)$ found in eight of the nine elements of $\boldsymbol{H}$ is numerically unstable.

One solution is to switch to an entirely new state vector when this condition occurs. Consider the equations mapping the state vector into the measurement space, summariesed in (24). The $\sqrt{(Rg\,\cos(\theta)\,\tan(|\phi|))}$ term found in each of the mappings is equivalent, through (3), to $|\boldsymbol{v}_{XY}|$. Since the velocities are treated as 'measurements' by the EKF that estimates orientation, $|\boldsymbol{v}_{XY}|$ is ideally suited to join the yaw and pitch in comprising the new state vector. Note that $\boldsymbol{v}_{XY}$ is in no way approximating the roll. A new set of mapping equations are required to transform this new state vector into the measurement space.

This solution poses two challenges. First, criteria for selecting the appropriate state model must be selected. Once this has been done, it is necessary to chose a method for initialising the new state after the state model has changed. Neither task is insurmountable. For example, Howland [2] tackles a similar problem through the creation of a manoeuvre threshold. Manoeuvres, or flight that is not straight-and-level, are only assumed to occur when a chosen manoeuvre parameter exceeds this manoeuvre threshold. When this occurs, the manoeuvre state model described in Section 3.2 is used. If the parameter is below the threshold, constant-velocity flight is assumed and the alternate state model, incorporating $|\boldsymbol{v}_{XY}|$ instead of $\phi$, is used. Furthermore, the relation between $|\boldsymbol{v}_{XY}|$ and $\phi$ leads to

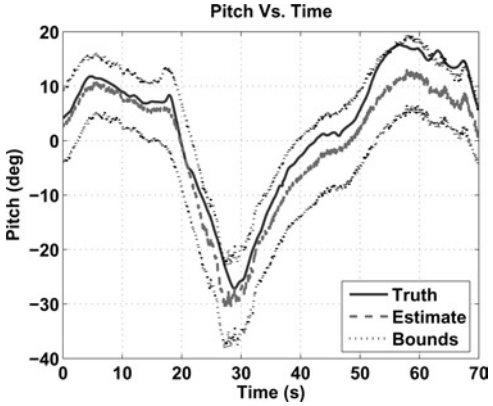


**Fig. 5** *Pitch estimated by the EKF: Edwards trajectory*

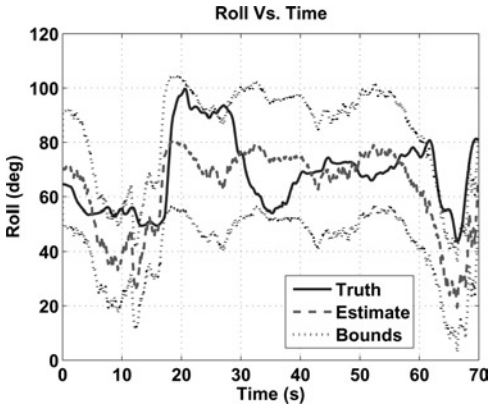


**Fig. 6** *Roll estimated by the EKF: Edwards trajectory*

natural initialisation procedures when a model switch occurs. When switching from the non-manoeuvre model to the manoeuvre model, $\phi$ is assumed to be transitioning away from zero, so zero is a natural initial value. When switching from the manoeuvre model to the non-manoeuvre model, the $|v_{XY}|$ state is initialised using the most recent measurement.

### 3.4 Solving for $\boldsymbol{h}$ and $\boldsymbol{H}$ under the non-manoeuvring model

If the non-manoeuvring model is selected, the nonlinear mapping of the state vector into the measurement space must change to reflect the new state vector. The new nonlinear mapping is given by

$$\boldsymbol{h}(x) = \begin{bmatrix} \boldsymbol{v}_X \\ \boldsymbol{v}_Y \\ \boldsymbol{v}_Z \end{bmatrix} = \begin{bmatrix} |\boldsymbol{v}_{XY}|\cos(\psi) \\ |\boldsymbol{v}_{XY}|\sin(\psi) \\ |\boldsymbol{v}_{XY}|\tan(\theta) \end{bmatrix} \tag{35}$$

and its linearisation matrix, $\boldsymbol{H}$, is given by

$$\boldsymbol{H} = \begin{bmatrix} \dfrac{\partial \boldsymbol{v}_X}{\partial \psi} & \dfrac{\partial \boldsymbol{v}_X}{\partial \theta} & \dfrac{\partial \boldsymbol{v}_X}{\partial |\boldsymbol{v}_{XY}|} \\ \dfrac{\partial \boldsymbol{v}_Y}{\partial \psi} & \dfrac{\partial \boldsymbol{v}_Y}{\partial \theta} & \dfrac{\partial \boldsymbol{v}_Y}{\partial |\boldsymbol{v}_{XY}|} \\ \dfrac{\partial \boldsymbol{v}_Z}{\partial \psi} & \dfrac{\partial \boldsymbol{v}_Z}{\partial \theta} & \dfrac{\partial \boldsymbol{v}_Z}{\partial |\boldsymbol{v}_{XY}|} \end{bmatrix} \tag{36}$$

or

$$\boldsymbol{H} = \begin{bmatrix} -|\boldsymbol{v}_{XY}|\,\sin(\psi) & 0 & \cos(\psi) \\ |\boldsymbol{v}_{XY}|\,\cos(\psi) & 0 & \sin(\psi) \\ 0 & |\boldsymbol{v}_{XY}|\,\sec^2(\theta) & \tan(\theta) \end{bmatrix} \tag{37}$$

## 4 Results

Two trajectories are used to demonstrate the EKF's performance. The first is a straight-and-level manoeuvre, while the second was recorded on-board a manoeuvring F-15 at Edwards Air Force Base [Note 2]. In both cases, Howland's EKF that estimates positions and velocities feeds 'measurements' to our EKF that estimates orientation. Using Howland's EKF to generate measurements is appropriate for the passive radar application described here, but could be replaced by some other means of generating velocity measurements to apply the technique to a different application.

Fig. 2 shows the yaw of the aircraft executing the straight-and-level manoeuvre, as well as $1-\sigma$ error bars obtained from the covariance matrix. Similar results involving aircraft pitch are shown in Fig. 3. Since the roll is assumed to be zero and is not estimated by the model when no acceleration is detected, it is neglected here. Note that the uncertainties in yaw and pitch are fairly small and stem almost entirely from the measurement noise. This is no longer the case when the aircraft executes the 'Edwards' manoeuvre. The error bars, shown in Figs. 4 through 6 for the roll, pitch and yaw, respectively, are appropriately larger now that the target accelerates. Although the estimated orientations are not always near the true values, the true values are usually within a standard deviation of the estimates.

## 5 Conclusions

Through the development of an EKF to estimate the aircraft's orientation, this paper makes two key contributions. First, the EKF provides a rigorous framework for estimating an aircraft's orientation from its velocity vector that blends the two distinct sources of error inherent to the problem. By incorporating modelling error into the estimate, it accounts for 'crabbing' and the slight deviations from coordianted flight that the pilot might induce. Second, the EKF supplements the estimated orientation with a measure of the uncertainty in that estimate. The two examples presented in Section 4 illustrate the EKF's ability to estimate aircraft orientation from velocity measurements whether the aircraft's trajectory is simple or complex.

Future work will seek to more thoroughly explore the issues of process noise tuning and covariance inflation in the EKF that estimates orientation. These two issues nearly always arise when designing an EKF, yet are frequently neglected in EKF literature. As is typically the case, we have tuned the EKF for our particular application using the training set of aircraft data at our disposal. To further develop the EKF in the future, we plan to use more extensive databases of aircraft data.

## 6 References

1 Ehrman, L., and Lanterman, A.: 'Automated target recogntion using passive radar and coordinated flight models'. Automatic Target Recognition XIII, Orlando, FL, April 2003, vol. SPIE Proc. 5094
2 Howland, P.E.: 'Target tracking using television-based bistatic radar', *IEE Proc., F: Radar Sonar Navigation*, 1999, **146**, (3), pp. 166–174
3 Howland, P.E.: 'Television-based bistatic radar', Ph.D thesis, University of Birmingham, England, 1997
4 Dole, C.E.: 'Flight theory and aerodynamics' (John Wiley & Sons, 1981)
5 Ehrman, L.M.: 'Automatic target recognition using passive radar and a coordinated flight model'. Master's thesis, School of Electrical and Computer Engineering, Georgia Institute of Technology, Atlanta, GA, 2003
6 Alessandri, A., Cuneo, M., Pagnan, S., and Sanguineti, M.: 'On the convergence of ekf-based parameters optimization for neural networks'. Proc. 42nd IEEE Conf., on Decision and Control, Maui, HI, December 2003, pp. 6181–6186

Note 2: The F-15C trajectory was obtained from the Joint Helmet Cuing System, Mission JH-16, conducted by the 445th Flight Test Squadron at Edwards Air Force Base in May 2000. Thanks to Major Larkin Hastriter and Lt. Col. Adam MacDonald for their assistance in obtaining this aircraft flight path.